JOURNAL OF GUIDANCE, CONTROL, AND DYNAMICS
Vol. 30, No. 4, July–August 2007

Optimal Multi-Objective Nonlinear Impulsive Rendezvous

Ya-Zhong Luo,* Yong-Jun Lei,† and Guo-Jin Tang‡
National University of Defense Technology, 410073 Changsha, People's Republic of China

DOI: 10.2514/1.27910

The multi-objective optimization of unperturbed two-body impulsive rendezvous is investigated in this paper. In addition to the total characteristic velocity and the time of rendezvous flight, the minimum relative distance between the chaser and the target in the chaser's free-flying path is proposed as another design performance index. The feasible iteration optimization model of three-objective impulsive rendezvous with path constraints including trajectory safety and field of view constraints is established using a Lambert algorithm. The multi-objective nondominated sorting genetic algorithm is employed to obtain the Pareto solution set. The −V-bar and +V-bar homing rendezvous missions are examined by the proposed approach. It is shown that tradeoffs between time of flight, propellant cost and passive trajectory safety, and several inherent principles of the rendezvous trajectory are demonstrated by this approach.

I. Introduction

THE optimal multiple-impulse rendezvous problem has been studied extensively. Prussing [1–3], Jones [4], Liu and Plexico [5], Carter and Brient [6], Carter and Alvarez [7], and Luo et al. [8] obtained optimal trajectories for impulsive rendezvous near a circular orbit using linearized equations. Lion and Handelsman [9], Jezewski and Rozendaal [10], Gross and Prussing [11], Taur et al. [12], Prussing [13], Prussing and Chiu [14], Kim and Spencer [15], Hughes et al. [16], and Shen and Tsiotras [17] obtained optimal trajectories for unperturbed two-body impulsive rendezvous. Jezewski [18], Haufler et al. [19], and Luo et al. [20] developed optimization approaches for perturbed and constrained rendezvous.

Several criteria need to be considered in rendezvous trajectory design, of which the total velocity characteristic is the typical measure of performance. However, the total velocity characteristic is not the single desired criterion and minimizing the time of flight serves as an equally attractive mission objective. In addition, trajectory safety is another important objective for designing a practical rendezvous mission, especially for an approach mission [21–24]. In this context, taking all these objectives into consideration and constructing a multi-objective optimization problem is very practical for operational rendezvous trajectory design. Although multi-objective optimization design technique has been widely used in many real-world optimization problems [25], it is less used in spacecraft trajectory design. Hartmann et al. [26] and Coverstone-Carroll et al. [27] reported the multi-objective optimization design of interplanetary spacecraft trajectories. Recently, Luo et al. [28] reported the multi-objective optimization of linearized rendezvous. The drawback of linearized rendezvous equations is that they are based upon the assumption of a linearized gravity field and a circular reference point orbit with no disturbing forces. As a result, they typically decrease in accuracy with increasing eccentricity, and with perturbing forces.

Although much work has been done on optimal impulsive rendezvous design, researches are seldom concerning on optimal rendezvous trajectory design with path constraints. Taur et al. [12] considered rendezvous and interception between coplanar circular orbits in an inverse-square gravitational field subject to a restricted class of interior path constraints, namely, minimum- and maximum-radius constraints. Primer vector theory was extended to incorporate path constraints, and the optimal number of impulses along with their times and positions were determined. Jezewski [18] extended the procedure of Taur et al. to general perturbed and constrained impulsive rendezvous. The analytical gradients with respect to objective function and constraints were formulated and the resulting parameter optimization problem was solved by a two-step approach using a gradient-based optimization algorithm. Jezewski's method was further improved by Haufler et al. [19] by adding various characteristic of operational constraints.

The objectives of this paper are twofold. First, to extend the multi-objective optimization technique of linearized impulsive rendezvous previously reported by the authors to optimal multi-objective nonlinear rendezvous design. Second, to include two path constraints including trajectory safety and field of view constraints which are operational for an approach mission into the multi-objective optimization design of rendezvous trajectory. The path constraints considered in [12,18] were emphasizing particularly on the phasing stage of rendezvous and their solution method was an indirect method based on the primer vector method and gradient-based optimization algorithm. The path constraints considered in this paper are for an approach mission and the constraints are handled by a genetic algorithm approach.

II. Multi-Impulse Rendezvous Using Lambert Solution

A. Multi-Impulse Rendezvous Problem

Given that the initial conditions for rendezvous are $\mathbf{r}_0$, $\mathbf{v}_0$, and t_0 and the final conditions, $\mathbf{r}_f$, $\mathbf{v}_f$, and t_f, the general dynamic equations are

$$\ddot{\mathbf{r}} = -\mu \frac{\mathbf{r}}{r^3} \tag{1}$$

Assuming an impulsive $\Delta\mathbf{v}_i$ is applied, the superscript $-$ indicates the state before an impulse, and $+$ indicates the state after an impulse. We get

$$\begin{cases} \mathbf{r}_i^+ = \mathbf{r}_i^- \\ t_i^+ = t_i^- \\ \Delta\mathbf{v}_i = \mathbf{v}_i^+ - \mathbf{v}_i^- \end{cases} \tag{2}$$

Without loss of generality, let

$$\mathbf{r}_i = \mathbf{r}_i^+ = \mathbf{r}_i^- \qquad t_i = t_i^+ = t_i^- \tag{3}$$

and assume $\mathbf{r}(t+\Delta t) = \mathbf{f}(\mathbf{r}(t), \mathbf{v}(t), t, t+\Delta t)$ and $\mathbf{v}(t+\Delta t) = \mathbf{g}(\mathbf{r}(t), \mathbf{v}(t), t, t+\Delta t)$ are the solutions to Eq. (1).

Received 19 September 2006; revision received 5 February 2007; accepted for publication 12 March 2007.

*Ph.D. Candidate, College of Aerospace and Material Engineering; yzluo@sohu.com. Student Member AIAA (Corresponding Author).
†Professor, College of Aerospace and Material Engineering.
‡Professor, College of Aerospace and Material Engineering.

For an intermediate impulse $i \neq 1$, $i \neq n$, where $n(\geq 2)$ is the number of impulses, the following conditions must be satisfied:

$$\mathbf{r}_i = \mathbf{f}(\mathbf{r}_{i-1}, \mathbf{v}_{i-1}^+, t_{i-1}, t_i) \qquad \mathbf{v}_i^- = \mathbf{g}(\mathbf{r}_{i-1}, \mathbf{v}_{i-1}^+, t_{i-1}, t_i) \tag{4}$$

The constraints corresponding to the initial conditions are given by

$$\mathbf{r}_1 = \mathbf{f}(\mathbf{r}_0, \mathbf{v}_0, t_0, t_1) \qquad \mathbf{v}_1^- = \mathbf{g}(\mathbf{r}_0, \mathbf{v}_0, t_0, t_1) \tag{5}$$

where t_1 is the time of the first impulse.

A similar set of constraints applied at the final conditions are given by

$$\mathbf{r}_n = \mathbf{f}(\mathbf{r}_f, \mathbf{v}_f, t_f, t_n) \qquad \mathbf{v}_n^+ = \mathbf{g}(\mathbf{r}_f, \mathbf{v}_f, t_f, t_n) \tag{6}$$

In summary, the general propellant-optimal multi-impulse rendezvous is to find $(\mathbf{r}_i, \mathbf{v}_i^+, \mathbf{v}_i^-, t_i)$, where $i = 1, 2, \ldots, n$ that satisfy the following constraints [16]:

$$\begin{cases} \mathbf{r}_1 = \mathbf{f}(\mathbf{r}_0, \mathbf{v}_0, t_0, t_1) \\ \mathbf{v}_1^- = \mathbf{g}(\mathbf{r}_0, \mathbf{v}_0, t_0, t_1) \\ \mathbf{r}_i = \mathbf{f}(\mathbf{r}_{i-1}, \mathbf{v}_{i-1}^+, t_{i-1}, t_i) \\ \mathbf{v}_i^- = \mathbf{g}(\mathbf{r}_{i-1}, \mathbf{v}_{i-1}^+, t_{i-1}, t_i) \\ \mathbf{r}_n = \mathbf{f}(\mathbf{r}_f, \mathbf{v}_f, t_f, t_n) \\ \mathbf{v}_n^+ = \mathbf{g}(\mathbf{r}_f, \mathbf{v}_f, t_f, t_n) \end{cases} \tag{7}$$

and to minimize the total velocity characteristic

$$J = \Delta v = \sum_{i=1}^{n} |\Delta \mathbf{v}_i| \tag{8}$$

B. Optimization Model with Feasible-Solution Iteration

The parameter optimization methods to the optimization problem described by Eqs. (7) and (8) can be divided into two categories called the feasible iteration approach and the infeasible iteration approach [16]. In the feasible iteration approach, each evaluation of the objective function produces a feasible solution that satisfies implicitly the rendezvous conditions. The feasible iteration approach requires a careful choice of the independent variables, while in the infeasible iteration approach, there is less restriction on the choice of independent variables. In the infeasible iteration approach, the rendezvous conditions are not necessarily satisfied for each objective function evaluation. The rendezvous conditions are satisfied upon convergence of the numerical optimization algorithm. Thus, in the infeasible iteration approach the constraints must be defined carefully, and the optimization algorithm must be able to handle nonlinear constraints. Hughes et al. [16] discussed details on how to formulate the optimization model of the feasible iteration approach. The applied optimization model of the feasible iteration approach is as follows.

The chosen independent variables, that is, the optimization variables are impulse times and the first $n-2$ impulse vectors:

$$t_i, \qquad i = 1, 2, \ldots, n \qquad \Delta \mathbf{v}_j, \qquad j = 1, 2, \ldots, n-2 \tag{9}$$

where $\Delta \mathbf{v}_i = (\Delta v_{Ii}, \Delta v_{Ji}, \Delta v_{Ki})$ is an impulse imposed on the chaser at time t_i, and it is expressed in Cartesian coordinates.

Calculating $\mathbf{r}_1$ and $\mathbf{v}_1^-$ in Eq. (5), and $\mathbf{r}_n$ and $\mathbf{v}_n^+$ in Eq. (6), we have

$$\begin{cases} \mathbf{v}_i^+ = \mathbf{v}_i^- + \Delta \mathbf{v}_i \\ \mathbf{r}_{i+1} = \mathbf{f}(\mathbf{r}_i, \mathbf{v}_i^+, t_i, t_{i+1}) \quad (i = 1, 2, \ldots, n-2) \\ \mathbf{v}_{i+1}^- = \mathbf{g}(\mathbf{r}_i, \mathbf{v}_i^+, t_i, t_{i+1}) \end{cases} \tag{10}$$

The terminal rendezvous conditions are satisfied by solving a Lambert problem Lambert$(\mathbf{r}_{n-1}, \mathbf{r}_n, t_n - t_{n-1})$.

III. Trajectory Safety Performance

A rendezvous mission can be divided into a number of major phases: launch, phasing, far-range rendezvous (homing rendezvous), close-range rendezvous, and docking [21]. The discussions concerning trajectory safety concentrate on the rendezvous phase, because the mission phase of launch and phasing are generally controlled by operators or computer functions on the ground. Generally, two categories are considered in rendezvous trajectory safety: active trajectory protection and passive trajectory protection. Active trajectory protection focuses on designing a closed loop guidance, navigation, and control (GNC) system and an approximate active collision avoidance maneuver (CAM), and more details on this issue can be found in [21]. On the other hand, passive trajectory protection concentrates on designing all trajectory elements in an approach trajectory sequence such that if, at any point of the trajectory, thrust control ceases, the resulting "free trajectory" will remain collision free for TBD (to be defined) time. In our optimal multi-objective rendezvous design, only passive trajectory protection is considered.

Assume that control ceases at time $\tau_0 (t_0 \leq \tau_0 \leq t_f)$ during the rendezvous trajectory with the chaser state $(\mathbf{r}_{\tau_0}^{\text{cha}}, \mathbf{v}_{\tau_0}^{\text{cha}})$ and the target state $(\mathbf{r}_{\tau_0}^{\text{tar}}, \mathbf{v}_{\tau_0}^{\text{tar}})$. In the free-flying path, the position vector of the chaser and the target at arbitrary time are given by

$$\mathbf{r}_{\tau_0}^{\text{cha}}(\tau) = \mathbf{f}(\mathbf{r}_{\tau_0}^{\text{cha}}, \mathbf{v}_{\tau_0}^{\text{cha}}, \tau_0, \tau), \qquad \mathbf{r}_{\tau_0}^{\text{tar}}(\tau) = \mathbf{f}(\mathbf{r}_{\tau_0}^{\text{tar}}, \mathbf{v}_{\tau_0}^{\text{tar}}, \tau_0, \tau) \tag{11}$$

where $\tau_0 \leq \tau \leq \tau_0 + \text{TBD}$.

We define the relative distance between the chaser and the target as

$$r(\tau) = |\mathbf{r}_{\tau_0}^{\text{cha}}(\tau) - \mathbf{r}_{\tau_0}^{\text{tar}}(\tau)| \tag{12}$$

The minimum value of $r(\tau)$ is used to measure whether the drift trajectory is safe or not

$$r_{\min}(\tau_0) = \min_{\tau_0 \leq \tau \leq \tau_0 + \text{TBD}} r(\tau) \tag{13}$$

$r_{\min}(\tau_0)$ can be calculated by numerically integrating the dynamic equations of the chaser and the target. As mathematical integration is required, this method is not efficient. A simplified analytical technique to quickly determine $r_{\min}(\tau_0)$ using linearized rendezvous equations has been proposed in [28] and this technique is simply summarized in the Appendix.

The rendezvous trajectory has a time history from t_0 to t_f, thus τ_0 can be any point in the range of $t_0 \leq \tau_0 \leq t_f$. We define r_{safe}

$$r_{\text{safe}} = \min_{t_0 \leq \tau_0 \leq t_f} r_{\min}(\tau_0) \tag{14}$$

r_{safe} is regarded as the trajectory safety performance index. From the point of view of optimal design, r_{safe} should be as large as possible. Therefore, r_{safe} is proposed as one design optimization objective function in the multi-objective rendezvous trajectory design

$$\max J = r_{\text{safe}} \tag{15}$$

Through Eq. (14), the calculation of r_{safe} involves two functional optimization problems. After $r_{\min}(\tau_0)$ is defined, one simplified method is used to calculate r_{safe}. Choose l points $(\tau_{0,1}, \tau_{0,2}, \ldots, \tau_{0,l})$ in the range of $[t_0, t_f]$ at equal intervals and calculate $r_{\min}(\tau_{0,i})$, then

$$r_{\text{safe}} = \min(r_{\min}(\tau_{0,1}), \ldots, r_{\min}(\tau_{0,l})) \tag{16}$$

IV. Multi-Objective Optimization Model

A. Objective Function Vector

The time of flight is the first objective function

$$\min f_1(\mathbf{x}) = t_f - t_0 \tag{17}$$

In this study, $t_0 = 0$.

The total velocity characteristic is chosen as the second objective function

$$\min f_2(\mathbf{x}) = \Delta v = \sum_{i=1}^{n} |\Delta \mathbf{v}_i| \tag{18}$$

The third objective function is the trajectory safety performance index

$$\min f_3(\mathbf{x}) = -r_{\text{safe}} \tag{19}$$

B. Optimization Variables

Because this is a minimum-time rendezvous, t_f is an optimization variable. The impulse times $t_i (i = 1, 2, \ldots, n)$ are also optimization variables. To improve optimization performance, the variable-scaling method is imposed on t_i. Let

$$\alpha_i = t_i / t_f \qquad 0 \le \alpha_i \le 1 \tag{20}$$

The Lambert algorithm is employed to naturally satisfy the terminal rendezvous conditions, that is, the impulse vector is defined by $t_i (i = 1, 2, \ldots, n)$, $\Delta \mathbf{v}_j (j = 1, 2, \ldots, n-2)$.

In total, the optimization variable vector includes three parts: one is t_f, the second part is $(\alpha_1, \ldots, \alpha_n)^T$, and the third part is $\Delta \mathbf{v}_j (j = 1, 2, \ldots, n-2)$.

C. Constraints

The constraints with respect to impulse times are considered. The general constraint on $t_i (i = 1, 2, \ldots, n)$ is

$$t_0 \le t_1 < t_2 \cdots < t_N \le t_f \tag{21}$$

For the practical rendezvous mission, it is necessary to adjust the vehicle's attitude before firing the engine, and this requirement constrains the interval time between two arbitrary impulses. The constraint is formulated as follows:

$$t_{i+1} - t_i \ge \Delta t \qquad (i = 1, 2, \ldots, n-1) \tag{22}$$

where Δt is a defined time interval. For a general passive-safety required rendezvous trajectory, r_{safe} should be larger than a defined value. This constraint is formulated by

$$r_{\text{safe}} - r^0_{\text{safe}} \ge 0 \tag{23}$$

where r^0_{safe} is a required safe range, which must be larger than 0. When $r^0_{\text{safe}} = 0$, it denotes no trajectory safety constraint.

For a practical rendezvous mission, the optical sensors, for example, camera and laser range finder types, have an additional operational constraint for the approach trajectory design, that is, a limited field of view (FOV) [21]. This puts limits on the lateral extension of the trajectory. An example of a −V-bar rendezvous is shown in Fig. 1. The x–y coordinate system is the same as that defined in Fig. A1, and the curvilinear orbit direction in shown as a straight line and is named V-bar after the orbital velocity vector $\mathbf{v}$; −V-bar denotes an opposite direction to V-bar.

Define the line-of-sight angle of the chaser with respect to the target as

$$\theta(t) = a \tan(|y(t)/x(t)|) \tag{24}$$

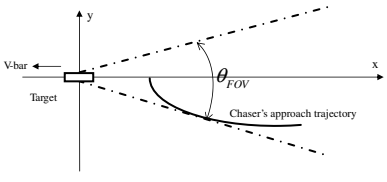

Fig. 1 Required field of view for a −V-bar rendezvous trajectory.

Thus, the FOV constraint can be formulated as

$$\theta_m = \max_{t_0 \le t \le t_f} \theta(t) \le \theta_{\text{FOV}}/2 \tag{25}$$

One simplified method is used to calculate θ_m. Choose m points $(t_1, t_2, \ldots, t_m)$ in the range of $[t_0, t_f]$ at equal intervals and calculate $\theta(t_i)$, then θ_m is given by

$$\theta_m = \max(\theta(t_1), \ldots, \theta(t_m)) \tag{26}$$

V. Multi-Objective Genetic Algorithms

A. MOGA

GAs (genetic algorithms) are global search methods that mimic the behavior observed in biological populations. GAs employ the principle of survival of the fittest in their search processes and have been applied successfully to the design of many complex systems. To perform the optimization process, GAs employ three operators to propagate the population of possible parameter values from one generation to the next one: "selection" operator, "crossover" operator, and "mutation" operator.

MOGA is an extended GA for multi-objective optimization. GAs solve a single-objective optimization problem by emulating the natural evolutionary process in which a population of design points (or individuals) is iteratively evolved to reach an optimum solution. In GAs, at each iteration, the probability that an individual is selected to evolve is governed by its fitness value, which is a function of that individual's single-objective value and its constraint values. MOGA extends a GA's fitness assignment method so that it is applicable to multiple objectives [25].

There are many variants of MOGA reported in the literature [25]. Among these MOGAs, the nondominated sorting genetic algorithm (NSGA) developed by Srinivas and Deb [29] is widely used. Hartmann et al. [26] and Coverstone-Carroll et al. [27] have successfully applied the NSGA to generate fronts of Pareto-optimal trajectories for both Earth–Mars and Earth–Mercury missions. NSGA-II [30] was advanced from its origin, NSGA. In NSGA-II, a fast-nondominated sorting approach is used for each individual to create Pareto rank, and a crowding distance assignment is applied to implement density estimations. In the next section, the model of the NSGA-II used in our study is presented.

B. Brief Description of the NSGA-II

The algorithm is based on the idea of transforming the m objectives to a single fitness measure by the creation of a number of fronts, sorted according to nondomination. During the fitness assignment, the first front is created as the set of solutions that is not dominated by any solutions in the population. These solutions are given the highest fitness and temporarily removed from the population, then a second nondominated front consisting of the solutions that are now nondominated is built and assigned the second-highest fitness, etc. This is repeated until each of the solutions has been assigned a fitness. After each front has been created, its members are assigned crowding distances (normalized distance to closest neighbors in the front in the objective space) later to be used for niching. More details of the NSGA-II are provided in [25,30].

The real-coded method is adopted in this paper. Unlike the original edition of NSGA-II, the arithmetical crossover operator and the nonuniform mutation operator [31] are applied. Selection is performed in tournaments of size two: the solution with the lowest front number wins. If the solutions come from the same front, the solution with the highest crowding distance wins, since a high distance to the closest neighbors indicates that the solution is located at a sparse part of the front. As for the constraint handling method, the method proposed by Deb et al. [30] is adopted in this multi-objective optimization. Feasible, noninferior designs are stored in an approximate Pareto set that is updated after each generation as new designs dominating previously stored designs are found.

VI. Results

A. Problem Configuration

In this paper, homing rendezvous missions are selected to demonstrate our approach. Homing rendezvous can also be called the far range rendezvous [21]. The major objective of the homing rendezvous phase is the reduction of trajectory dispersions, that is, the achievement of position, velocity, and angular rate conditions, which are necessary for the initiation of close-range rendezvous operations. Passive trajectory safety is one important performance index for designing the homing rendezvous trajectory [21]. The homing rendezvous typically starts at a range of a few ten kilometers and ends at a range of a few kilometers from the target in one less orbital revolution. It can be categorized as a near coplanar circular rendezvous problem and a two-impulse Hohmann transfer is always the simplest and propellant-optimal solution [21]. However, as requirements for compensating navigation and guidance errors, the number of homing rendezvous maneuvers is required to be larger than 2, for example, the maneuver number of the Space Shuttle Orbiter and the Soyuz/Progress homing rendezvous is 3 or 4 [21]. Thus, we examine the homing rendezvous with three and four impulses, respectively. Two representative homing rendezvous trajectories are analyzed and compared: the −V-bar and +V-bar trajectories. The former requires the chaser enter a position-hold point behind the target, and a position-hold point ahead of the target applies to the latter. The target orbit is a near circular orbit with apogee height of 355 km and perigee height of 340 km. The −V-bar and +V-bar homing rendezvous have the same initial conditions:

$$\mathbf{X}_0 = (35713.3\ \text{m}, -13455.1\ \text{m}, -28.8\ \text{m}, -22.9\ \text{m/s}, 0.66\ \text{m/s}, -0.09\ \text{m/s})^T$$

The final conditions for the −V-bar homing rendezvous are $\mathbf{X}_f = (2000\ \text{m}, 0, 0, 0, 0, 0)^T$ and for the +V-bar homing rendezvous are $\mathbf{X}_f = (-2000\ \text{m}, 0, 0, 0, 0, 0)^T$.

The parameters of the NSGA-II are the population size 100, the maximum number of generations 200, the probability of crossover 0.92, and the probability of mutation 0.10. $l = 10$, $m = 10$, $\Delta t = 100$ s. The NSGA-II is used to optimize the three- and four-impulse, −V-bar and V-bar homing rendezvous, with trajectory safety constraint ($r^0_{\text{safe}} = 1500$ m) and without trajectory safety constraint ($r^0_{\text{safe}} = 0$), and with FOV constraint ($\theta_{\text{FOV}} = 100$ deg) and without FOV constraint ($\theta_{\text{FOV}} = 180$ deg), respectively. Considering the stochastic characteristic of the NSGA-II, 10 independent runs for each test case are completed, and all of the Pareto-optimal solutions obtained in 10 runs are compared and revised by deleting the inferior and repeating solutions. Then the revised Pareto-optimal solutions of 10 runs are regarded as the final Pareto solution set.

Table 1 Statistical results on the number of Pareto-optimal solutions of three-impulse −V-bar

Problem	No. of Pareto-optimal solutions		
	Maximum	Minimum	Mean
$r^0_{\text{safe}} = 0$, $\theta_{\text{FOV}} = 180$ deg	586	166	373.9
$r^0_{\text{safe}} = 1500$ m, $\theta_{\text{FOV}} = 180$ deg	323	125	242.5
$r^0_{\text{safe}} = 0$, $\theta_{\text{FOV}} = 100$ deg	318	153	196.7

B. Three-Impulse Results

Table 1 shows the statistical results on the number of converged Pareto-optimal solutions obtained in each execution for the −V-bar homing rendezvous. Table 2 lists three Pareto-optimal solutions of the three-impulse +V-bar homing rendezvous without safety constraint. Figures 2 and 3 illustrate and compare several selected Pareto-optimal fronts, in which converged Pareto-optimal solutions are indicted with an "o" and a "+."

Figure 4 illustrates the normal and free-flying trajectories corresponding with the first solution listed in Table 2. $\widehat{AC}$ in Fig. 4 is the normal trajectory, and r_{safe} is obtained when control ceases during the second and the third impulses. As the third impulse is imposed nearly at the final time, the free-flying trajectory is also passing through the destination B, and the free-flying trajectory is denoted by $\widehat{BCD}$ in Fig. 4 (starts at 1582 s).

C. Four-Impulse Results

Table 3 shows the statistical results on the number of converged Pareto-optimal solutions obtained in each execution for the four-impulse −V-bar homing rendezvous. Table 4 lists three Pareto-optimal solutions of the four-impulse −V-bar homing rendezvous without trajectory safety and FOV constraints. Figure 5 compares the Pareto-optimal fronts of +V-bar and −V-bar four-impulse with trajectory safety constraint. Figure 6 compares the Pareto-optimal fronts of four- and three-impulse −V-bar rendezvous without path constraints. Figure 7 illustrates the normal and free-flying trajectories corresponding with the first solution listed in Table 4. $\widehat{AC}$ in Fig. 7 is the normal trajectory, r_{safe} is obtained when control ceases during the second impulse and the third impulse, and the free-flying trajectory is denoted by $\widehat{BD}$ in Fig. 7 (starts at 1433.8 s).

r_{safe} for the three-impulse case in Fig. 3 and four-impulse in Fig. 7 is calculated as 559 and 1333 m, respectively, using linearized rendezvous equations. By numerically integrating the chaser and target two-body orbits, they are calculated as 579 and 1335 m, respectively. Our experiments show that the simplified technique for calculating the safety range has an error of less than 5%; it can reduce time cost by 15 times. In a CPU 2.9 Ghz computer, the integration method consumes 1000 s, while only 100 s for the analytical method.

D. Pareto Optimality Verification

Tables 1–4 and Figs. 2–7 have reported some Pareto solutions obtained by the NSGA-II. However, at this time their Pareto optimality has not been verified. In this section, we will show partially the Pareto optimality of the solutions by comparing them with the propellant-optimal solutions. Based on Lawden's necessary conditions for an optimal impulsive trajectory [32], Lion and Handelsman [9] formulated the procedures for obtaining the propellant-optimal solution for nonlinear time-fixed rendezvous, which had been applied by Jezewski and Rozendaal [10], Gross and Prussing [11], and Prussing and Chiu [14]. As Lawden's necessary conditions and Lion and Handelsman's procedure are applied to free trajectory, −V-bar homing rendezvous without path constraints ($r^0_{\text{safe}} = 0$ and $\theta_{\text{FOV}} = 180$ deg) is selected as examples to test the Pareto optimality.

Let t_f vary in [1000, 5000] s at the interval of 100 s, and solve each corresponding time-fixed propellant-optimal solution using a global parallel simulated annealing algorithm [33] and the nonoptimal primer vector theory developed by Lion and Handelsman [9] which is used to determine an optimal number of impulses. We find that a two-impulse solution is optimal for $1000 < t_f < 2800$ s, for

Table 2 Three Pareto-optimal solutions of three-impulse +V-bar ($r^0_{\text{safe}} = 0$ and $\theta_{\text{FOV}} = 180$ deg)

Index	Optimization variables		Objective function value		
	$\alpha_i (i = 1, 2, 3)$	$\Delta\mathbf{v}_1$, m/s	t_f, s	Δv, m/s	r_{safe}, m
1	0.243, 0.495, 0.997	[−0.768, −4.388, 2.180]	2895.460	10.297	559.076
2	0.140, 0.471, 0.989	[1.402, −5.351, 2.595]	1015.703	89.172	1365.974
3	0.069, 0.515, 0.998	[1.530, −6.263, 1.868]	2043.663	17.858	1896.341

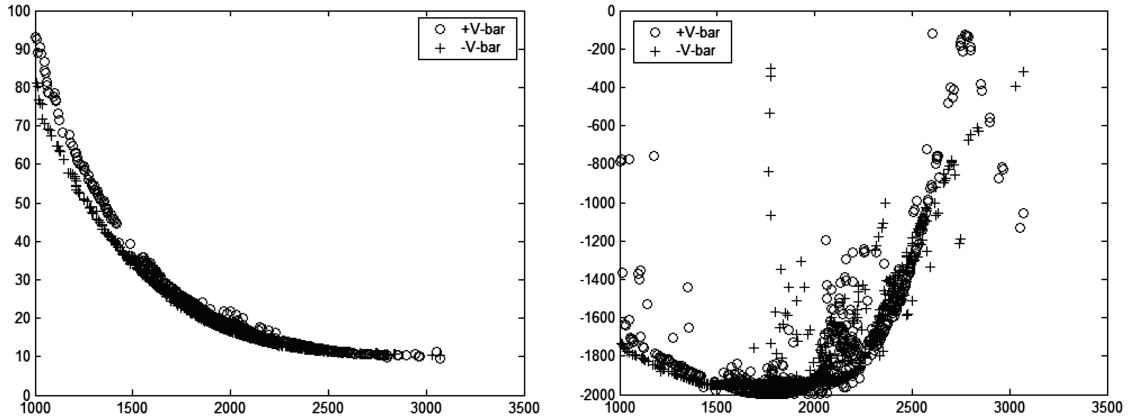

a) Δv (m/s) vs $t_f(s)$ b) $-r_{safe}$ (m) vs $t_f(s)$

Fig. 2 Pareto-optimal fronts of three-impulse ($r^0_{\text{safe}} = 0$ and $\theta_{\text{FOV}} = 180$ deg).

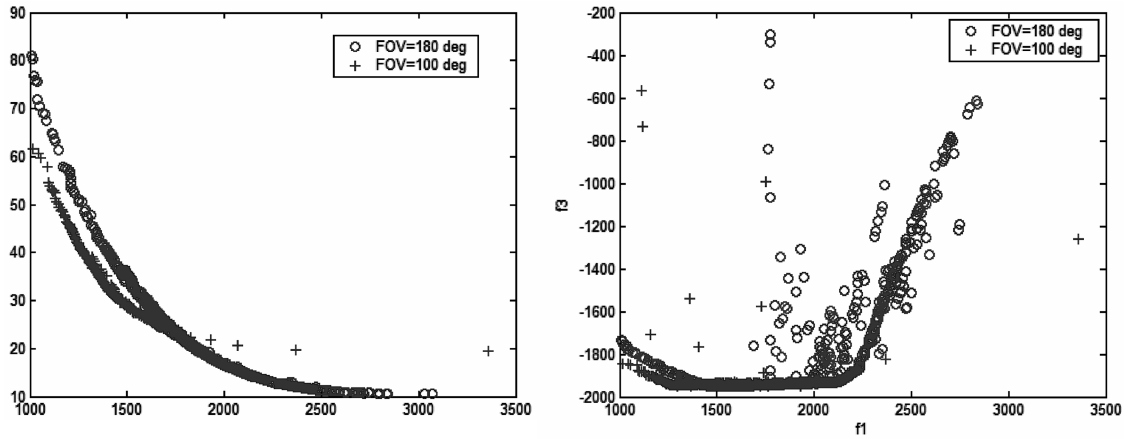

a) Δv (m/s) vs $t_f(s)$ b) $-r_{safe}$ (m) vs $t_f(s)$

Fig. 3 Pareto-optimal fronts of three-impulse −V-bar ($r^0_{\text{safe}} = 0$).

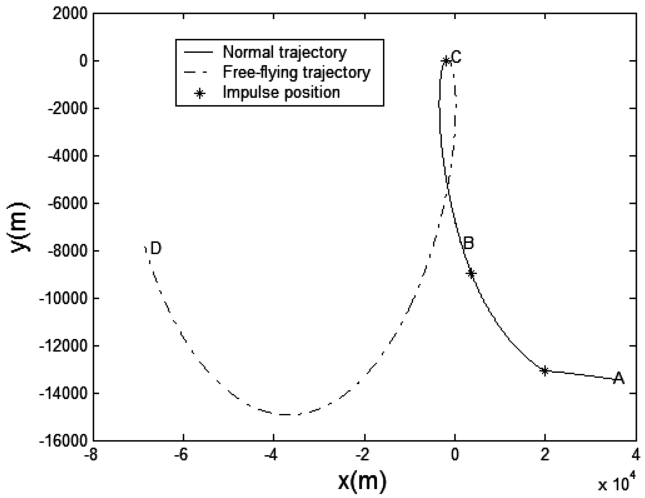

Fig. 4 The chaser's normal and free-flying trajectories in the *x*–*y* plane (the first solution listed in Table 2).

example, in Fig. 8a the primer vector magnitude time history satisfies Lawden's necessary conditions. Whereas the two-impulse solution is not the optimal for $2800 \leq t_f \leq 5000$ s, for example, in Fig. 8b the primer vector magnitude time history violates Lawden's necessary conditions. As the nonoptimal primer vector theory demonstrates [9], an additional impulse and a coasting trajectory are required to obtain the propellant-optimal solution for this case. Figure 8c illustrates the primer vector magnitude time history of the three-impulse solution, and it satisfies Lawden's necessary conditions. This is true for the cases of $2800 < t_f \leq 5000$ s.

Figure 9 compares the relation between Δv and t_f of Pareto-optimal and propellant-optimal solutions. It shows that the Pareto-optimal solutions illustrate the similar trend between Δv and t_f as the propellant-optimal solutions do. Besides, the propellant-optimal solutions demonstrate that for $t_f > 2800$ s, Δv reduces very small as t_f increases. In accordance with this pecularity, the Pareto-optimal solutions concentrate on the range of t_f in [1000, 2800] s.

The homing rendezvous is similar as the cases of coplanar rendezvous in the vicinity of a circular orbit investigated by Prussing [1,2]. Prussing concluded that the propellant-optimal solution was a two-impulse or three-impulse solution for transfer time of one less orbital revolution (see Figs. 8–10 of [2]). Based on Prussing's conclusions, it can be declared that the three-impulse is better than the four-impulse in terms of propellant cost for the homing rendezvous completed in one less orbital revolution. The results provided in this paper can give an exemplification for this issue.

Table 3 Statistical results on the number of Pareto-optimal solutions of four-impulse −V-bar

	No. of Pareto-optimal solutions		
Problem	Maximum	Minimum	Mean
$r^0_{\text{safe}} = 0$, $\theta_{\text{FOV}} = 180$ deg	447	119	224.3
$r^0_{\text{safe}} = 1500$ m, $\theta_{\text{FOV}} = 180$ deg	238	66	122.2

Table 4 Three Pareto-optimal solutions of four-impulse −V-bar ($r^0_{\text{safe}} = 0$ and $\theta_{\text{FOV}} = 180$ deg)

	Optimization variables			Objective function value		
Index	$\alpha_i (i = 1, 2, 3, 4)$, s	$\Delta\mathbf{v}_1$, m/s	$\Delta\mathbf{v}_2$, m/s	t_f, s	Δv, m/s	r_{safe}, m
1	0.226, 0.497, 0.601, 0.989	$(-0.541, -3.686, 4.710)$	$[0.0358, -0.302, -0.651]^T$	2582.785	13.871	1335.588
2	0.269, 0.519, 0.636, 0.996	$(-1.629, -3.801, 2.716)$	$[0.153, -2.355, 1.471]^T$	1176.067	73.800	1771.006
3	0.235, 0.517, 0.649, 0.998	$[-2.565, -5.867, 1.392]^T$	$[2.929, -0.750, 2.468]^T$	1771.005	25.734	1959.109

E. Discussion

According to the data provided by Tables 1–4 and Figs. 2–9, we can conclude the following:

1) There is an obvious relation between the time of flight and the total characteristic velocity: the longer rendezvous time would result in less propellant cost and vice versa. However, the relation is not apparent between the time of fight (or the total characteristic velocity) and the trajectory safety performance index.

2) The −V-bar homing rendezvous has better passive trajectory safety performance than the +V-bar homing rendezvous. For the same time of rendezvous, the −V-bar rendezvous has less propellant cost compared with the +V-bar rendezvous, which can be explained by the latter needing to fly a great range.

3) For the same time of rendezvous, the three-impulse rendezvous has less propellant cost than the four-impulse. This is the same as Prussing's results about coplanar rendezvous in the vicinity of a circular orbit when the transfer time is limited to less than one orbital revolution.

4) The fronts with and without path constraints including trajectory safety and FOV constraints have no evident difference. However, the number of Pareto-optimal solutions without path constraints is evidently larger than that with. Besides, adding the trajectory safety constraint does not result in an increment of propellant cost, while the introduction of FOV constraint results in more propellant cost.

The first three peculiarities are the same as those observed in the multi-objective optimization of linearized rendezvous [28]. The last peculiarity regards the path-constrained rendezvous trajectory which is not considered in [28]. As only a single set of initial conditions is considered, these observations would not always be true for other cases. However, they may also be useful for other cases. Besides, our approach would be competent if it is necessary to observe generalizations for other cases. One run on a 2.9 GHz CPU computer requires about 100 s. The approach is efficient and effective to provide very valuable insights into the tradeoffs available in the design space of rendezvous trajectory.

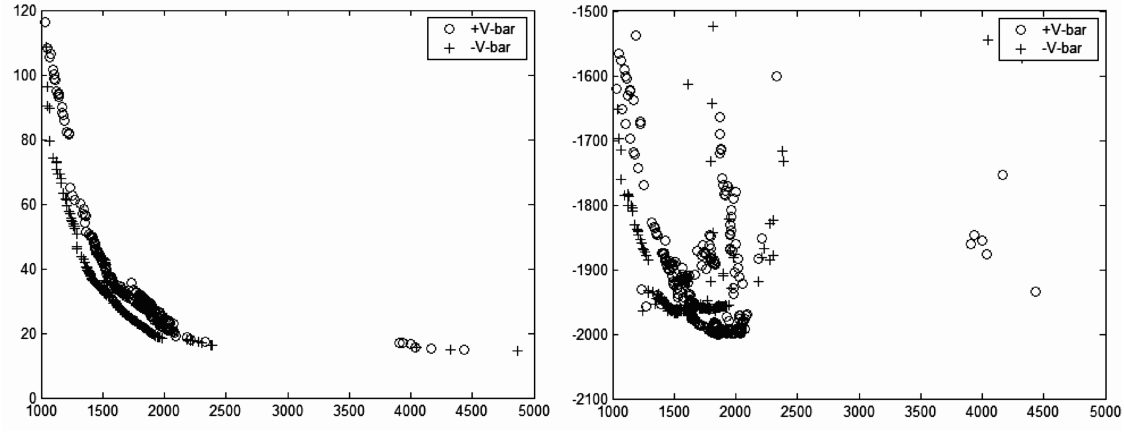

a) Δv (m/s) vs $t_f(s)$ **b) $-r_{safe}$ (m) vs $t_f(s)$**

Fig. 5 Pareto-optimal fronts of four-impulse ($r^0_{\text{safe}} = 1500$ m and $\theta_{\text{FOV}} = 180$ deg).

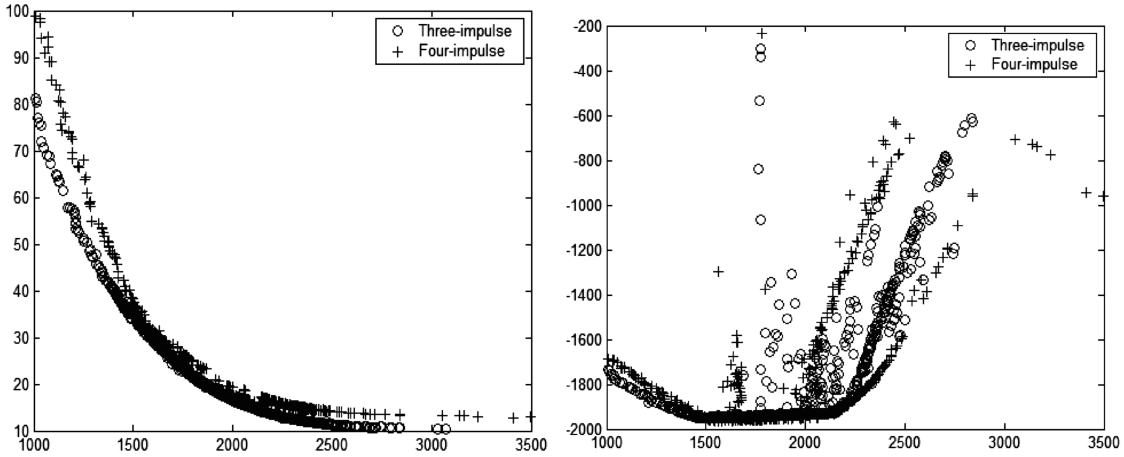

a) Δv (m/s) vs $t_f(s)$ **b) $-r_{safe}$ (m) vs $t_f(s)$**

Fig. 6 Pareto-optimal fronts of −V-bar ($r^0_{\text{safe}} = 0$ and $\theta_{\text{FOV}} = 180$ deg).

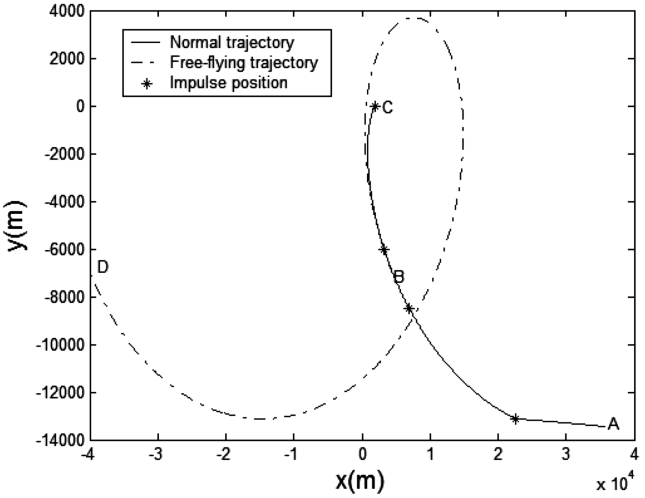

Fig. 7 The chaser's normal and free-flying trajectories in the *x*–*y* plane (the first solution listed in Table 4).

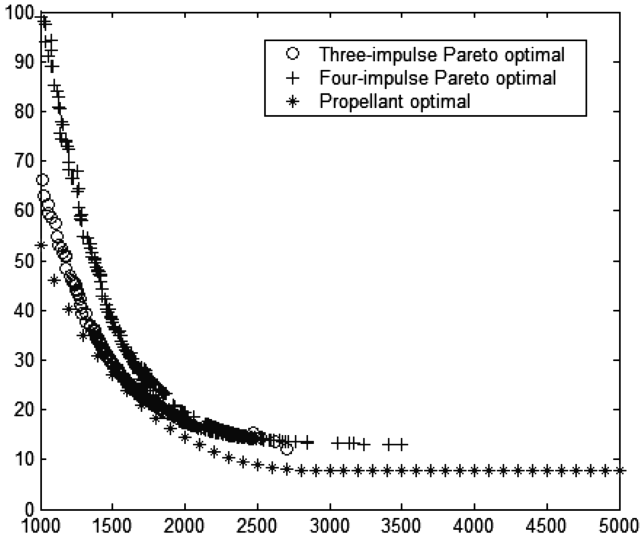

Fig. 9 Comparisons of Δv (m/s) vs t_f (s) between Pareto-optimal and propellant-optimal solutions of −V-bar ($r^0_{\text{safe}} = 0$ and $\theta_{\text{FOV}} = 180$ deg).

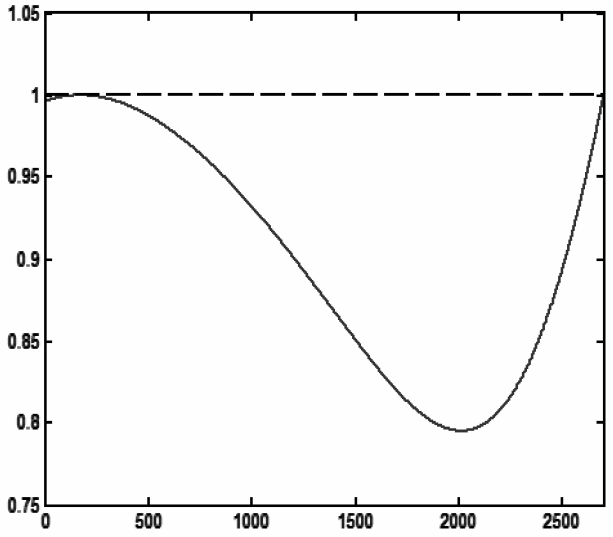

a) Two-impulse, $t_f = 2700\ s$ ($t_1 = 137.6\ s$, $t_2 = 2700\ s$)

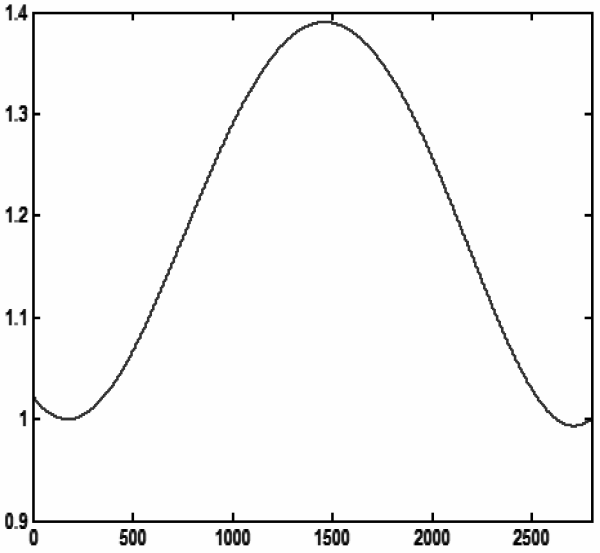

b) Two-impulse, $t_f = 2800\ s$ ($t_1 = 183.4\ s$, $t_2 = 2800\ s$)

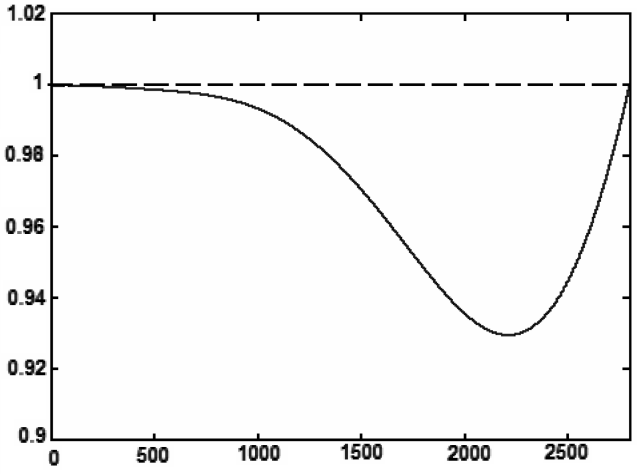

c) Three-impulse, $t_f = 2800\ s$ ($t_1 = 88.4\ s$, $t_2 = 350.4\ s$, $t_3 = 2800\ s$)

Fig. 8 Primer vector magnitude of −V-bar rendezvous.

$$\begin{cases} x(\tau) = \left(x_{\tau 0} + \frac{2\dot{y}_{\tau 0}}{\omega}\right) + 2\left(\frac{2\dot{x}_{\tau 0}}{\omega} - 3y_{\tau 0}\right)\sin(\omega\Delta\tau) - 2\frac{\dot{y}_{\tau 0}}{\omega}\cos(\omega\Delta\tau) - (3\dot{x}_{\tau 0} - 6\omega y_{\tau 0})\Delta\tau \\ y(\tau) = \left(4y_{\tau 0} - 2\frac{\dot{x}_{\tau 0}}{\omega}\right) + \frac{\dot{y}_{\tau 0}}{\omega}\sin(\omega\Delta\tau) - \left(3y_{\tau 0} - 2\frac{\dot{x}_{\tau 0}}{\omega}\right)\cos(\omega\Delta\tau) \\ z(\tau) = \frac{\dot{z}_{\tau 0}}{\omega}\sin(\omega\Delta\tau) + z_0\cos(\omega\Delta\tau) \end{cases} \tag{A2}$$

where $\Delta\tau = \tau - \tau_0$.

Compared with the linearized rendezvous which is subjected to circular and near rendezvous, the two-body nonlinear multi-objective model is more accurate and suitable to more problems. However, the model in this study still does not include the perturbations such as J_2 and atmospheric drag, which are necessary for the operational missions. Future work should investigate the multi-objective optimization of the perturbed rendezvous problem. As the requirement of obtaining a solution set, it is very important for the NSGA-II to locate one feasible solution easily. In this study, the introduction of the Lambert algorithm makes each solution during iteration satisfy the rendezvous condition naturally, which mainly contributes to the success of the NSGA-II. At this time, there is no easy and quick method to provide one feasible solution for the perturbed rendezvous. Thus, the critical work for multi-objective optimization of the perturbed rendezvous is to design an efficient method to locate a feasible solution for the perturbed rendezvous.

VII. Conclusions

The present optimal nonlinear two-body impulsive rendezvous design incorporates three objective functions including the minimum propellant cost, the minimum time of flight, and the maximum trajectory safety performance index. The introduction of a Lambert algorithm makes the NSGA-II locate a Pareto-optimal solution set easily. Our studies provide an efficient and effective tool to demonstrate the relation between the time of flight, the propellant cost, and the passive trajectory safety for rendezvous trajectory. Besides, the proposed approach is able to analyze and compare different rendezvous missions with different rendezvous schemes, a different number of impulses, without or with path constraints, etc. By identifying multiple solutions, the approach has produced a variety of missions to meet different needs.

Appendix: Simplified Technique to Calculate the Minimum Relative Distance

The relative dynamics motion for rendezvous is illustrated by the well-known Clohessy–Wiltshire (CW) equations, which is set up in a rotating orbit coordinate frame that is fixed to the target spacecraft as show in Fig. A1.

$$\left.\begin{array}{c} \ddot{x} - 2\omega\dot{y} = u_x \\ \ddot{y} + 2\omega\dot{x} - 3\omega^2 y = u_y \\ \ddot{z} + \omega^2 z = u_z \end{array}\right\} \tag{A1}$$

where ω is the orbital rate of the target spacecraft, x, y, and z are the position components of the chase spacecraft, and u_x, u_y, and u_z are the acceleration components of the chase spacecraft.

Assume control ceases at any time $\tau_0 (t_0 \le \tau_0 \le t_f)$ during the rendezvous trajectory. Based on the CW equations, the chaser's free-flying position at time τ is found to be the analytical function of the initial position vector $\mathbf{X}_{\tau 0} = (x_{\tau 0}, y_{\tau 0}, z_{\tau 0})$ and the initial velocity vector $\dot{\mathbf{X}}_{\tau 0} = (\dot{x}_{\tau 0}, \dot{y}_{\tau 0}, \dot{z}_{\tau 0})^T$ at time τ_0

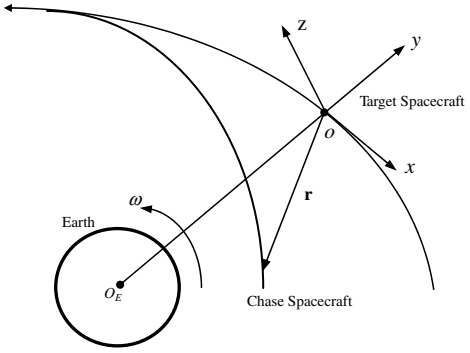

Fig. A1 Orbit coordinate system.

The corresponding velocity is found to be

$$\begin{cases} \dot{x}(\tau) = 2(2\dot{x}_{\tau 0} - 3y_{\tau 0}\omega)\cos(\omega\Delta\tau) + 2\dot{y}_{\tau 0}\sin(\omega\Delta\tau) - 3\dot{x}_{\tau 0} + 6\omega y_{\tau 0} \\ \dot{y}(\tau) = \dot{y}_{\tau 0}\cos(\omega\Delta\tau) + (3\omega y_{\tau 0} - 2\dot{x}_{\tau 0})\sin(\omega\Delta\tau) \\ \dot{z}(\tau) = \dot{z}_{\tau 0}\cos(\omega\Delta\tau) - z_{\tau 0}\omega\sin(\omega\Delta\tau) \end{cases} \tag{A3}$$

The corresponding acceleration is found to be

$$\begin{cases} \ddot{x}(\tau) = 2\omega(3y_{\tau 0}\omega - 2\dot{x}_{\tau 0})\sin(\omega\Delta\tau) + 2\omega\dot{y}_{\tau 0}\cos(\omega\Delta\tau) \\ \ddot{y}(\tau) = -\omega\dot{y}_{\tau 0}\sin(\omega\Delta\tau) + \omega(3\omega y_{\tau 0} - 2\dot{x}_{\tau 0})\cos(\omega\Delta\tau) \\ \ddot{z}(\tau) = -\omega\dot{z}_{\tau 0}\sin(\omega\Delta\tau) - z_{\tau 0}\omega^2\cos(\omega\Delta\tau) \end{cases} \tag{A4}$$

The relative distance of the chaser to the target in time τ is defined as

$$r(\tau) = f(\mathbf{x}_{\tau 0}, \dot{\mathbf{x}}_{\tau 0}, \tau_0, \tau) = \sqrt{x(\tau)^2 + y(\tau)^2 + z(\tau)^2} \tag{A5}$$

The minimum value of $r(\tau)$ is defined as

$$r_{\min}(\tau_0) = \min_{\tau_0 \le \tau \le \tau_0 + \mathrm{TBD}} r(\tau) \tag{A6}$$

In the study, TBD is set as the period of the target orbit.

Assuming $r(\tau)$ gets its minimum at time τ^*, τ^* should satisfy the following two conditions:

$$\frac{dr}{d\tau^*} = 0, \qquad \frac{d^2 r}{d\tau^{*2}} > 0 \tag{A7}$$

From Eqs. (A3–A5), it is

$$\frac{dr}{d\tau} = (x\dot{x} + y\dot{y} + z\dot{z})/r \tag{A8}$$

$$\frac{d^2r}{d\tau^2} = -\frac{(x\dot{x}+y\dot{y}+z\dot{z})^2}{r^3} + \frac{\dot{x}^2+x\ddot{x}+\dot{y}^2+y\ddot{y}+\dot{z}^2+z\ddot{z}}{r} \quad \text{(A9)}$$

If $\frac{dr}{d\tau} = 0$, Eq. (A9) is revised as

$$\frac{d^2r}{d\tau^2} = \frac{\dot{x}^2+x\ddot{x}+\dot{y}^2+y\ddot{y}+\dot{z}^2+z\ddot{z}}{r} \quad \text{(A10)}$$

Based on the above analyses, the iteration method to calculate $r_{\min}(\tau_0)$ is described as follows:

Step 1: give an initial guess τ^0, and iteration $= 0$.

Step 2: solve $dr/d\tau = 0$ by the Newton–Raphson method and obtain one solution τ^*.

Step 3: if $d^2r/d\tau^{*2} > 0$, τ^* is the true solution, ends; otherwise, go to step 4.

Step 4: let $\tau^0 = (\tau^* + \tau^0)/2$, iteration$+ = 1$. if iteration$<$ iterationmax, go to step 2; otherwise go to step 5.

Step 5: make $\tau^* = \tau^0$ as the true solution.

Acknowledgments

The paper is supported by the China Postdoctoral Science Foundation (Ref. 20060390892), the Science Project of the National University of Defense Technology (Ref. JC06-01-01), and the Ph.D. Programs Foundation of Ministry of Education of China (Ref. 20069998002).

References

[1] Prussing, J. E., "Optimal Four-Impulse Fixed-Time Rendezvous in the Vicinity of a Circular Orbit," *AIAA Journal*, Vol. 7, No. 5, 1969, pp. 928–935.

[2] Prussing, J. E., "Optimal Two- and Three-Impulse Fixed-Time Rendezvous in the Vicinity of a Circular Orbit," *AIAA Journal*, Vol. 8, No. 7, 1970, pp. 1221–1228.

[3] Prussing, J. E., "Optimal Impulsive Linear Systems: Sufficient Conditions and Maximum Number of Impulses," *Journal of the Astronautical Sciences*, Vol. 43, No. 2, 1995, pp. 195–206.

[4] Jones, J. B., "Optimal Rendezvous in the Neighborhood of a Circular Orbit," *Journal of the Astronautical Sciences*, Vol. 24, No. 1, 1976, pp. 55–90.

[5] Liu, F. C., and Plexico, L. D., "Improved Solution of Optimal Impulsive Time-Fixed Rendezvous," *Journal of Spacecraft and Rockets*, Vol. 19, No. 6, 1982, pp. 521–528.

[6] Carter, T. E., and Brient, J., "Linearized Impulsive Rendezvous Problem," *Journal of Optimization Theory and Applications*, Vol. 86, No. 3, 1995, pp. 553–584.

[7] Carter, T. E., and Alvarez, S. A., "Quadratic-Based Computation of Four-Impulse Optimal Rendezvous Near Circular Orbit," *Journal of Guidance, Control, and Dynamics*, Vol. 23, No. 1, 2000, pp. 109–117.

[8] Luo, Y. Z., Tang, G. J., and Li, H. Y., "Optimization of Multiple-Impulse Minimum-Time Rendezvous with Impulse Constraints Using a Hybrid Genetic Algorithm," *Aerospace Science and Technology*, Vol. 10, No. 6, 2006, pp. 534–540.

[9] Lion, P. M., and Handelsman, M., "Primer Vector on Fixed-Time Impulsive Trajectories," *AIAA Journal*, Vol. 6, No. 1, 1968, pp. 127–132.

[10] Jezewski, D. J., and Rozendaal, H. L., "An Efficient Method for Calculating Optimal Free-Space N-Impulse Trajectories," *AIAA Journal*, Vol. 6, No. 11, 1968, pp. 2160–2165.

[11] Gross, L. R., and Prussing, J. E., "Optimal Multiple-Impulse Direct Ascent Fixed-Time Rendezvous," *AIAA Journal*, Vol. 12, No. 7, 1974, pp. 885–889.

[12] Taur, D. R., Coverstone-Carroll, V., and Prussing, J. E., "Optimal Impulse Time-Fixed Orbital Rendezvous and Interception with Path Constraints," *Journal of Guidance, Control, and Dynamics*, Vol. 18, No. 1, 1995, pp. 54–60; also AIAA Paper 90-2972, 20–23 Aug. 1990.

[13] Prussing, J. E., "A Class of Optimal Two-Impulse Rendezvous Using Multiple-Revolution Lambert Solutions," *Journal of the Astronautical Sciences*, Vol. 48, No. 2, 2000, pp. 131–148.

[14] Prussing, J. E., and Chiu, J. H., "Optimal Multiple-Impulse Time-Fixed Rendezvous Between Circular Orbits, "*Journal of Guidance, Control, and Dynamics*, Vol. 9, No. 1, 1986, pp. 17–22.

[15] Kim, Y. H., and Spencer, D. B., "Optimal Spacecraft Rendezvous Using Genetic Algorithms," *Journal of Spacecraft and Rockets*, Vol. 39, No. 6, 2002, pp. 859–865.

[16] Hughes, S. P., Mailhe, L. M., and Guzman, J. J., "A Comparison of Trajectory Optimization Methods for the Impulsive Minimum Propellant Rendezvous Problem," *Advances in the Astronautical Sciences*, Vol. 113, 2003, pp. 85–104.

[17] Shen, H. J., and Tsiotras, P., "Optimal Two-Impulse Rendezvous Using Multiple-Revolution Lambert Solutions," *Journal of Guidance, Control, and Dynamics*, Vol. 26, No. 1, 2003, pp. 50–61.

[18] Jezewski, D. J., "Optimal Rendezvous Trajectories Subject to Arbitrary Perturbations and Constraints," AIAA Paper 92-4507-CP, 1992.

[19] Haufler, B. R., Jezewski, D. J., and Multder, T. A., "Operational Constraints in Optimal, Impulsive, Rendezvous Trajectories," AAS Paper 93-140, 1993.

[20] Luo, Y. Z., Tang, G. J., Wang, Z. G., and Li, H. Y., "Optimization of Perturbed and Constrained Fuel-Optimal Impulsive Rendezvous Using a Hybrid Approach," *Engineering Optimization*, Vol. 38, No. 8, 2006, pp. 959–973.

[21] Fehse, W., *Automated Rendezvous and Docking of Spacecraft*, Cambridge University Press, Cambridge, England, 2003.

[22] Suzaki, M., Shoda, K., and Ikeuchi, M., "Analysis and Planning for Precise Orbital Maneuvers," IAF Paper 92-0044, 1992.

[23] Marsh, S. M., and White, B. D., "Trajectory Design and Navigation Analysis for Cargo Transfer Vehicle Proximity Operations," AIAA Paper 92-4436-CP, 10–12 Aug. 1992.

[24] Roger, A. B., and MeInnes, C. R., "Safety Constrained Free-Flyer Path Planning at the International Space Station," *Journal of Guidance, Control, and Dynamics*, Vol. 23, No. 6, 2000, pp. 971–979.

[25] Deb, K., "Multi-Objective Optimization Using Evolutionary Algorithms," Wiley, LTD, Chichester, 2002, pp. 171–285.

[26] Hartmann, J. W., Coverstone-Carroll, V., and Williams, S. N., "Optimal Interplanetary Spacecraft Trajectories via a Pareto Genetic Algorithm," *Journal of the Astronautical Sciences*, Vol. 46, No. 3, 1998, pp. 267–282.

[27] Coverstone-Carroll, V., Hartmann, J. W., and Mason, W. J., "Optimal Multi-Objective Low-Thrust Spacecraft Trajectories," *Computer Methods in Applied Mechanics and Engineering*, Vol. 186, No. 2, 2000, pp. 387–402.

[28] Luo, Y. Z., Tang, G. J., and Lei, Y. J., "Optimal Multi-Objective Linearized Impulsive Rendezvous," *Journal of Guidance, Control, and Dynamics*, Vol. 30, No. 2, 2007, pp. 383–389.

[29] Srinivas, N., and Deb, K., "Multiobjective Function Optimization Using Nondominated Sorting Genetic Algorithms," *Evolutionary Computation*, Vol. 2, No. 3, 1995, pp. 221–248.

[30] Deb, K., Pratap, A., Agarwal, S., and Meyarivan, T., "A Fast and Elitist Multi-Objective Genetic Algorithm: NSGA-II," *IEEE Transactions on Evolutionary Computation*, Vol. 6, No. 2, 2000, pp. 182–197.

[31] Michalewicz, Z., Janikow, C., and Krawczyk, J., "A Modified Genetic Algorithm for Optimal Control Problem," *Computers and Mathematics with Applications*, Vol. 23, No. 2, 1992, pp. 83–94.

[32] Lawden, D. F., *Optimal Trajectories for Space Navigation*, Butterworths, London, 1963.

[33] Luo, Y. Z., and Tang, G. J., "Parallel Simulated Annealing Using Simplex Method," *AIAA Journal*, Vol. 44, No. 12, 2006, pp. 3143–3146.